A SWTM based aerodynamic testing apparatus for offshore floating wind turbines

Jiahuan Lin [a], Yangwei Wang [a], Huawei Duan [a], Yuanchang Liu [b] and Jun Zhang [a,*]

[a] *School of Mechanical Engineering and Automation, Fuzhou University, Fuzhou 350108, China*

[b] *Department of Mechanical Engineering, University College London, Torrington Place, London WC1E 7JE, UK*

Corresponding author: Jun Zhang (zhang_jun@fzu.edu.cn). School of Mechanical Engineering and Automation, Fuzhou University, Fuzhou 350108, China.

A SWTM based aerodynamic testing apparatus for offshore floating wind turbines

Abstract: In marine applications, the scaled wind turbine model (SWTM) based aerodynamic testing apparatus is regarded as one of the most effective approaches to predict the aerodynamic performance of offshore floating wind turbines (OFWTs). To fully disclose the aerodynamics of OFWTs, such kind of apparatus should meet two design requirements: 1) accurate representation of the aerodynamic characteristics of reference wind turbines and 2) reasonable reproduction of the environmental factors from real-world wind-wave-coupled field. Baring with these considerations, the authors propose a cost-effective SWTM based aerodynamic testing apparatus, which consists of an innovative SWTM, a wind-wave simulator (WWS), and a data acquisition and analyses system. The proposed SWTM is featured by a double-deck tower, which satisfies the requirements of similarity in geometry, stiffness, and mass, and a set of redesigned blades. The proposed WWS is capable of simulating both the time-varying inflow wind and the wave-induced platform motions through a wind field generator and a motion simulator. Based on the developed apparatus, a series of aerodynamic tests are conducted to validate the effectiveness of the apparatus design. In addition, the coupling effects of inflow wind and platform motions on aerodynamics of OFWT are further revealed through experimental tests.

Keywords: scaled wind turbine model, wind-wave simulator, double-deck tower, redesigned blade, aerodynamic tests

1. INTRODUCTION

With the soaring requirement for renewable energy utilization, offshore floating wind turbines (OFWTs) have gained wide attentions from both academic and industrial communities in recent years. Among the OFWT developing techniques, the design of OFWTs and the layout arrangement of wind farms both require accurate aerodynamic prediction (Goupee et al. 2012, Liu et al. 2019, Porté-Agel et al. 2020). However, predicting aerodynamics of OFWTs is a difficult task because of complicated inflow wind and uncontrollable wave-induced platform motions as well. There are three commonly used ways in predicting aerodynamics of OFWTs, i.e. analytical calculation, numerical simulation, and experimental testing. Among them, experimental testing is the most reliable method, which may also provide crucial evidences for analytical calculation and numerical simulation (Nielsen et al. 2006, Ahn and Shin 2019, Yang et al. 2021). Despite its merit of reliability, experiment testing for OFWTs has great challenges due to high testing cost, uncontrolled environmental factors (Simandjuntak et al. 2021, Tchertchian and Millet 2022), and incomplete

reproducibility of structural properties. As an alternative solution, scaled wind turbine model (SWTM) based aerodynamic testing apparatus has been proposed and adopted by both academic and industrial communities.

A SWTM based aerodynamic testing apparatus usually consists of three subsystems, i.e. SWTM, wind-wave simulator (WWS), and data acquisition and analyses system (DAAS). Since the DAAS has been well developed in the past decades, the design of SWTM and WWS are two critical issues in developing such kind of experimental testing apparatus.

As to the first issue of SWTM design, a number of efforts have been conducted. For example, Wen et al. (2019) designed a SWTM of a 5MW wind turbine with a hollow conical tower by following the scaling laws of geometry, kinematics, and the Froude factors. They further proposed two rotor designs to enhance the thrust performance of the SWTM (Wen et al. 2020). By taking more parameters into account, Martin et al. (2011, 2014) designed a new SWTM with a hollow multi-stage cylindrical tower and a redesigned blade for better performance. Later, Duan et al. (2016a) proposed a thrust-matched blade system and carried out an experimental comparison with the scaled blade system. There is a common thread in these studies in that the basic parameters of an SWTM are firstly determined according to traditional scaling laws and then used as guidelines to design the mechatronics structures and aerodynamic structures. It needs to point out that in these studies the tower of SWTMs cannot meet the requirements of stiffness similarity and geometry similarity simultaneously. Besides, the power performance is often ignored when redesigning the blade system in these studies. In order to design a SWTM which can fully represent the aerodynamic features of the original reference wind turbine (RWT), the above two shortcomings in the previous studies should be avoided. From this perspective, in the present study, a new scaling strategy is used to design the tower of SWTM and the power performance is taken into account when redesigning the blade system.

As to the second issue of WWS design, some efficacious efforts have also been conducted. These efforts can roughly be classified into two groups. The first group focused on the wind field generator. For example, Belloli et al. (2020) utilized a wind tunnel to provide experimental wind field for the tests of an

SWTM. Du et al. (2016) generated a controllable wind field by 9 fans to test the performance of a new blade. Fowler et al. (2013) constructed a wind generation system with 6 industrial fans to generate the required wind field for aerodynamics testing. As can be seen from these studies, the wind field generator system is usually designed as a multi-fan system. The second group emphasized the reproduction of wave-induced platform motions. There are two ways in realizing this: one is basin-wave-platform simulator, the other is motion simulator. For example, Chen et al. (2018) carried out some model tests for two different conceptual blades in the Shanghai Jiao Tong University Deep-water Offshore Basin. Duan et al. (2016b) carried out a model test of a spar OFWT in the towing tank of Shanghai Jiao Tong University. Bayati et al. (2014) designed a motion simulator and verified it by a motion task related to a 5MW OFWT nominal operating condition. Compared with the basin-wave-platform experiment, the motion simulator has the advantages of lower manufacturing cost and less space requirement.

This paper aims to provide an economic yet efficient SWTM based aerodynamic testing apparatus. Based on the above discussions, the fundamental idea is to design an innovative SWTM to represent the aerodynamic properties of the RWT and to develop a WWS to reproduce a controllable coupling wind-wave field. For the design of the innovative SWTM, a double-deck tower structure is proposed to satisfy the requirements of stiffness similarity and geometry similarity simultaneously. Meanwhile, a redesigned blade is designed for better aerodynamic performance. For the development of WWS, an array of industrial axial fans is constructed as the wind field generator to produce the desired wind field and a six-degree-of-freedom (6-DOF) parallel manipulator is utilized as the motion simulator to generate the wave-induced platform motions for the SWTM. To validate the feasibility of the proposed design, some basic experimental tests are carried out. After that, a set of experimental tests are conducted to reveal the coupling effects of inflow wind and platform motions on aerodynamics of an OFWT.

The rest of the paper is organized as follows. In Section 2, the SWTM based aerodynamic testing apparatus is designed and fabricated. In Section 3, some aerodynamic tests are carried out on the SWTM based apparatus. In Section 4, some conclusions are drawn to close the study.

2. Design of SWTM based aerodynamic testing apparatus

2.1. Design of parameters

For the sake of generality, a NREL-5MW wind turbine is chosen as the RWT. To design a SWTM on this basis, it is necessary to determine the scaling laws. Among the present researches, the major view is that it should be based on the Froude scaling law, the scaling law of geometry and their derivative scaling laws, such as scaling laws of stiffness and mass (Lin et al. 2022a, Martin et al. 2014). Following these laws, the geometric scaling factors can be used to derive the scaling factors of other parameters. According to the recommendation of the International Marine Engineering Community, the geometric scaling factor λ between the RWT and the SWTM is generally set as 60-80 (Yang J M, Xiao L F 2008). In the present study, λ is selected as 80. Based on this geometric scaling factor, the basic parameters of the RWT, the scaling factors (Robertson et al. 2014, Jonkman et al. 2009, Ruzzo et al. 2021) and the basic parameters of the SWTM are shown in Table 1. Based on these parameters, the mechatronics design and the aerodynamics design of the SWTM are conducted in the next subsections.

Table 1 The basic parameters of the RWT, the scaling factors and the basic parameters of the SWTM.

Parameters	Prototype	Scaling factor	Model
Rated power	5 MW	$\lambda^{3.5}$	1.09 W
Rotor diameter	126 m	λ	1575 mm
Hub height	90 m	λ	1125 mm
Rated wind speed	11.4 m/s	$\lambda^{0.5}$	1.275 m/s
Rated rotor speed	12.1 rpm	$\lambda^{-0.5}$	108.2 rpm
Rotor thrust	800 kN	λ^{3}	1.56 N
Tower length	87.6 m	λ	1095 mm
Tower upper diameter	3.87 m	λ	48.38 mm
Tower lower diameter	6 m	λ	75 mm
Tower stiffness	2.61×10^{11} N·m^2	λ^{5}	79.65 N·m^2
Nacelle mass	240000 kg	λ^{3}	468.75 g
Tower mass	347460 kg	λ^{3}	678.63 g

2.2. Mechatronic design

The mechatronics design mainly involves the design of the tower, the nacelle and the hub. The following contexts will illustrate the details of the mechatronics design.

2.2.1. Tower

As shown in Table 1, the mass of the model tower should meet the following requirement:

$$\frac{G_{\mathrm{p}}}{G_{\mathrm{m}}} = \lambda^3 \tag{1}$$

where G is the mass of tower; hereafter, the subscripts p and m denote the prototype and the model, respectively; λ is the geometric scaling factor.

To make the deformation and the natural frequency comply with the scaling requirement, the scaling law of stiffness should be met. Since the material of the model tower is different from that of the prototype, the stiffness requirement should be described as:

$$E_{\mathrm{m}} I_{\mathrm{m}} = \frac{E_{\mathrm{p}} I_{\mathrm{p}}}{\lambda^5} \tag{2}$$

where E is the elastic modulus of tower; I is the cross-section moment of inertia of tower.

Assuming the model tower is a hollow cylinder, then I_{m} can be described as:

$$I_{\mathrm{m}} = \frac{\pi\left(D_{\mathrm{m}}{}^4 - d_{\mathrm{m}}{}^4\right)}{64} \tag{3}$$

where D and d are the outer and inner diameters of the tower, respectively.

In such a way, the total mass of model tower can be calculated by:

$$G_{\mathrm{m}} = \rho_{\mathrm{tower}} \pi \frac{D_m^2 - d_m^2}{4} l \tag{4}$$

where, ρ_{tower} is the density of material of the model tower; l is the length of the model tower.

According to (1) to (4), there is no solution for the outer diameter D_{m} and inner diameter d_{m} of the model tower when λ=80. To solve this problem, a double-deck tower is proposed to satisfy the scaling law of

geometry, stiffness and mass simultaneously. The inner deck of the tower, which connected with the platform and the nacelle, is designed as a hollow cylindrical structure to meet the scaling law of stiffness. The outer deck of the tower, which connected with the platform, is designed as a hollow cone to meet the scaling law of geometry. Meanwhile, the total mass of the double-deck tower should be equal to the target value as calculated in Table 1. In order to reach the target mass of the tower, the material of the inner deck tower is chosen as aluminum alloy 6061. Following the stiffness calculation, the outer diameter of the inner deck is designed as 16 mm while the inner diameter of the inner deck is designed as 14 mm.

Since the outer deck of the model tower must satisfy the geometric scaling requirement and the overall mass constrain, there are the following design criteria:

$$\begin{cases} \dfrac{D_{\mathrm{p}}}{D_{\mathrm{m}}} = \lambda \\ G_{\mathrm{m,out}} = G_{\mathrm{m}} - G_{\mathrm{m,in}} \end{cases} \tag{5}$$

where $D_{\mathrm{m,out}}$ is the diameter of the outer deck tower; $G_{\mathrm{m,out}}$ is the mass of the outer deck tower; $G_{\mathrm{m,in}}$ is the mass of the inner deck tower. The material of outer deck tower is chosen as PA12. The structural design of the model tower is illustrated in Fig. 1.

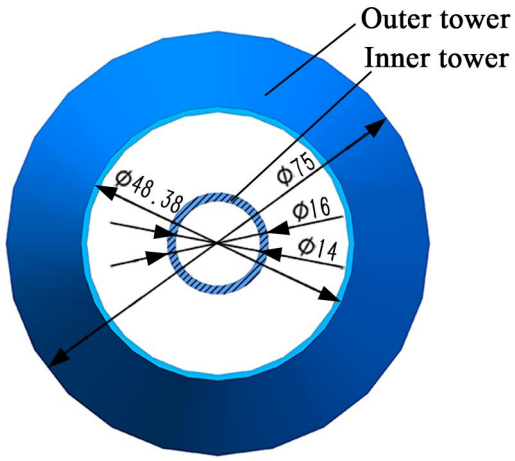

Fig. 1. The structure of model tower.

2.2.2. Nacelle and hub

The nacelle is designed as a combination of an adjustable tilt angle mechanism and an aluminum alloy drive-train unit. The adjustable tilt angle mechanism can adjusts the rotor within a range from 0° to 10°, and it is installed at the bottom of the drive-train unit. The drive-train unit consists of a servo motor, a torque sensor, a driving shaft, a pair of nylon gears, and a hollow main shaft. The servo motor is selected as CBL2040 to provide the expected rotor speed for the SWTM operating at desired Tip Speed Ratio (TSR). The torque sensor is selected as NC10E to measure the rotor torque. The nylon gear pair is designed with a transmission ratio of 1:1 (tooth number 30, module 1 mm). The main shaft is designed as hollow to allow the slip-ring cables passing through it, and it is directly connected to the hub through screw-nut assemblage. For clarity, Fig. 2 illustrates the exploded view and the physical structure of the nacelle.

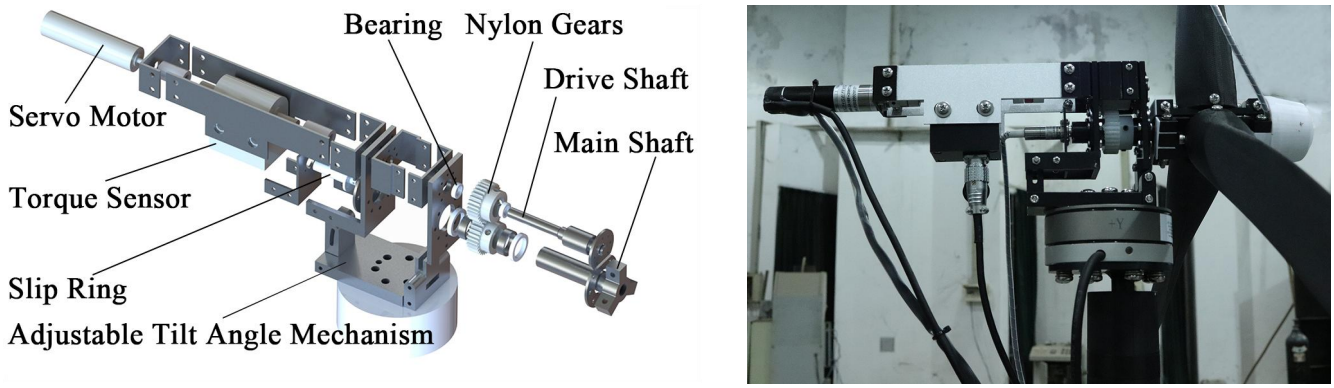

(a) (b)

Fig. 2. The nacelle (a) An exploded view. (b) The physical structure.

According to reference (Jonkman et al. 2009), the hub diameter of the RWT is set as 3.5 m. Thus, following the scaling law of geometry, the hub diameter of the SWTM can be calculated as 43.75 mm. Due to the structural limitation of the hub, a manual pitch control system is designed to replace the original electric pitch control system as shown in Fig. 3.

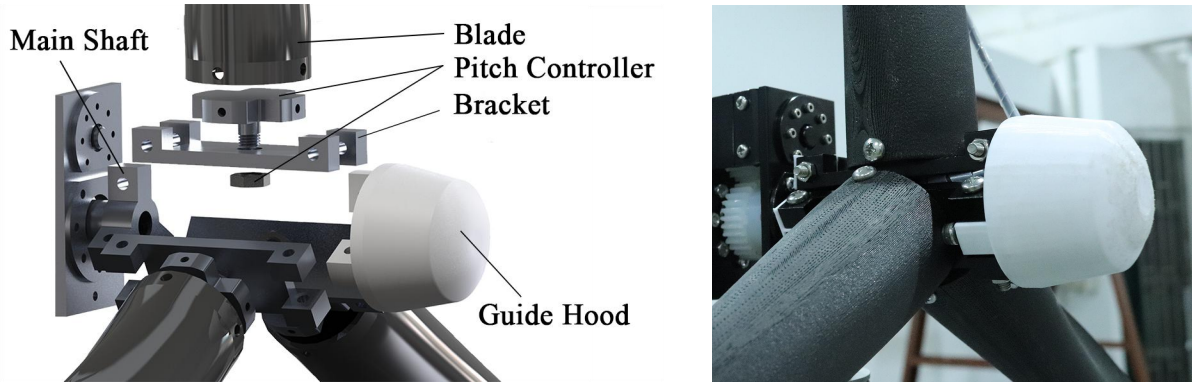

(a) (b)

Fig. 3. The hub (a) An exploded view. (b) The physical structure.

2.3. Aerodynamic design

The projection of airfoil section of the blade in the NREL-5MW RWT is shown in Fig. 4 (a), a detailed description can be found in (Jonkman et al. 2009). However, if this blade is directly scaled to design a model blade, the aerodynamic performance of the SWTM will be far lower than that of the RWT due to the Reynolds number effect (RNE) (Martin 2011, Martin et al. 2014). To be specific, the RNE will yield to a decreased lift coefficient and an increased drag coefficient of the original airfoils (Lin et al. 2022b). To avoid the RNE-aroused aerodynamic deficiency, the AG14 airfoil is selected in this study to improve the aerodynamic performance of the model blade, and its chords and twists are optimized to obtain a redesigned blade for better aerodynamic performance. The AG14 airfoil is a thin airfoil with a high lift coefficient and a low drag coefficient at low Reynolds number, making it suitable for the redesigned blade with the scaled Reynolds number, 1.6×10^4.

The aerodynamic performance is represented by the rotor thrust coefficient C_T and the power coefficient C_P. The thrust coefficient C_T and the power coefficient C_P are calculated by the definition of wind energy density (Li et al. 2013), and the formulas are as follows:

$$C_T = \frac{T_{rotor}}{\frac{1}{2}\rho_{air} V^2 A} \tag{6}$$

$$C_{\mathrm{P}} = \frac{P_{\mathrm{rotor}}}{\frac{1}{2}\rho_{\mathrm{air}} V^3 A} \tag{7}$$

where T_{rotor} is the rotor thrust; P_{rotor} is the power of the rotor; ρ_{air} is the density of air; V is the wind speed; A is the cross-sectional area of the effective wind field.

Based on the above definition, the optimization objective F is set as the follow:

$$F = \min\left((C_{\mathrm{T}} - C_{\mathrm{T,rated}}) + (C_{\mathrm{P}} - C_{\mathrm{P,rated}})\right) \tag{8}$$

where $C_{\mathrm{T,rated}}$ is the thrust coefficient of the RWT at rated TSR; $C_{\mathrm{P,rated}}$ is the power coefficient of the RWT at rated TSR.

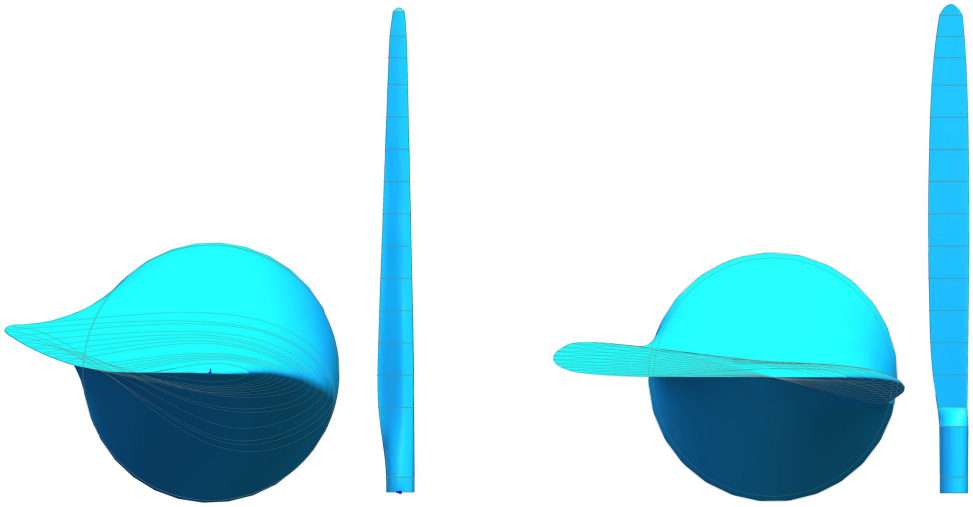

(a) (b)

Fig. 4. The projection of airfoil section of blades (a) The prototype blade. (b) The redesigned blade.

The above optimization problem can be solved with the pattern search algorithm. As the result, the chords and twists of the redesigned blade are shown in Table 2. For clarity, the projection of the airfoil section of the redesigned blade is shown in Fig. 4 (b).

Based on the blade element method (BEM), the aerodynamic performance of the prototype blade, the directly scaled blade and the redesigned blade can be calculated. The results are shown in Fig. 5.

Table 2 Chords and twists of the redesigned blade.

r/R	Chord/R	Twist	Airfoil
0.046	0.056	12.59	Cylinder
0.089	0.058	12.59	Cylinder
0.132	0.058	12.59	Cylinder
0.187	0.061	12.59	AG14
0.252	0.070	10.99	AG14
0.317	0.076	9.49	AG14
0.382	0.079	8.09	AG14
0.447	0.081	6.80	AG14
0.512	0.082	5.62	AG14
0.577	0.082	4.53	AG14
0.642	0.081	3.55	AG14
0.707	0.079	2.67	AG14
0.772	0.076	1.90	AG14
0.837	0.071	1.23	AG14
0.892	0.064	0.74	AG14
0.935	0.056	0.41	AG14
0.978	0.046	0.13	AG14

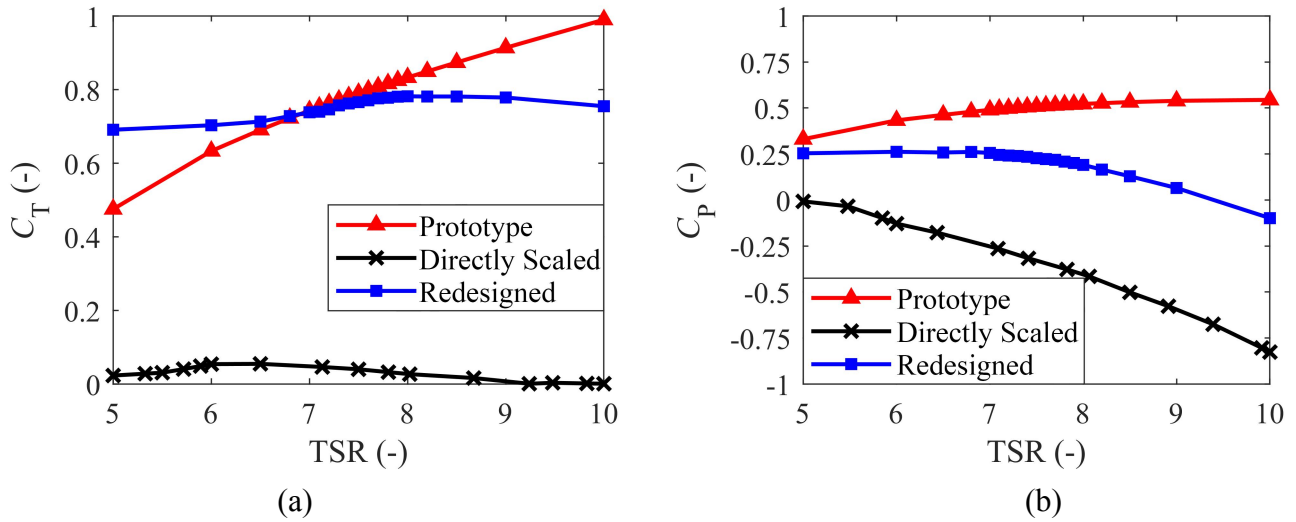

(a) (b)

Fig. 5. Comparison of different blades performance (a) The thrust coefficient. (b) The power coefficient.

In Fig. 5 (a), it reveals that the redesigned blade performs much better than the directly scaled blade in terms of the thrust coefficient. Also, it matches well with the prototype under the rated TSR of 7. In Fig. 5 (b), it can be observed that although the power coefficient of the redesigned blade is much higher than that of the directly scaled blade (which is negative, meaning the directly scaled blade does works back to the wind field), but it is still much lower than that of the prototype. This result is consistent with the prior research findings that there is an unbridgeable gap between the power coefficients of SWTM and prototype (Martin et al. 2014,

Lin 2022c). Therefore, the above optimized aerodynamic performance of the model blade maybe the limit result of the SWTM under rated TSR.

For practical engineering applications, it is preferable that the rotor thrust should be firstly guaranteed during the OFWT model tests. Nevertheless, the above analyses manifest that the redesigned blade is reasonable as it can reproduces similar aerodynamics of the RWT.

2.4. WWS design

The WWS includes a wind field generator and a motions simulator. The following contexts will introduce the design details of the two function modules.

2.4.1. Wind field generator

A wind field generator is designed to be consisting of 12 axial flow fans installed in a 3×4 rectangular frame, which is shown in Fig.6. The gross specifications of the axial flow fans are listed in Table 3. These fans are controlled by 3 inverters, and each inverter connected with 4 fans to generate a uniform wind flow or a vertical wind shear. Besides, a transfer cover and a screen are installed in front of the axial fans to reduce the turbulence intensity. The maximum wind speed of this wind field generator is 8 m/s. A coordinate system is shown in Fig. 6, where z=0 denotes the center height of wind field generator, as well as the hub height of the SWTM.

Table 3 Specifications of the axial flow fans.

Item	Specifications
Power	2.2 kW
Air flow	17200 m^3/h
Rotate speed	1450 rpm
Wind pressure	251 Pa

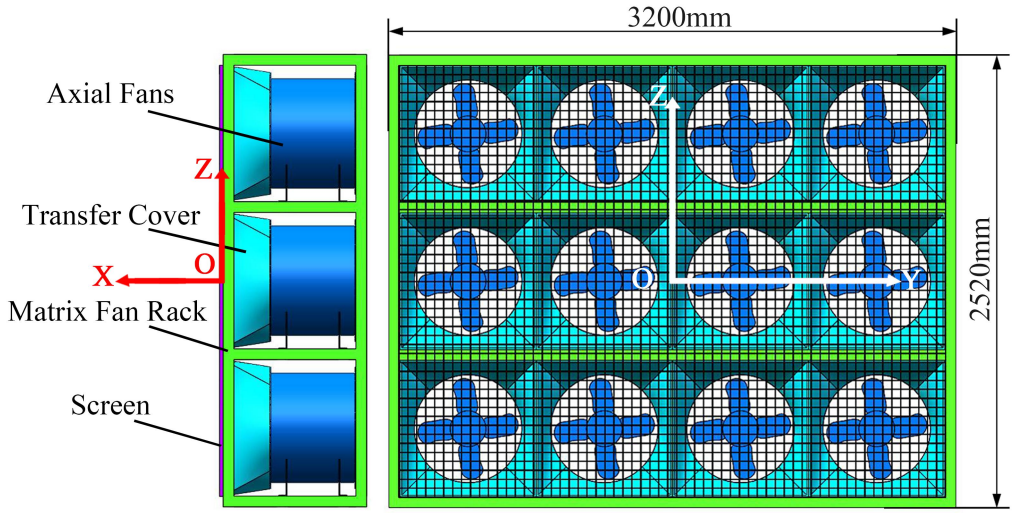

Fig. 6. Wind field generator.

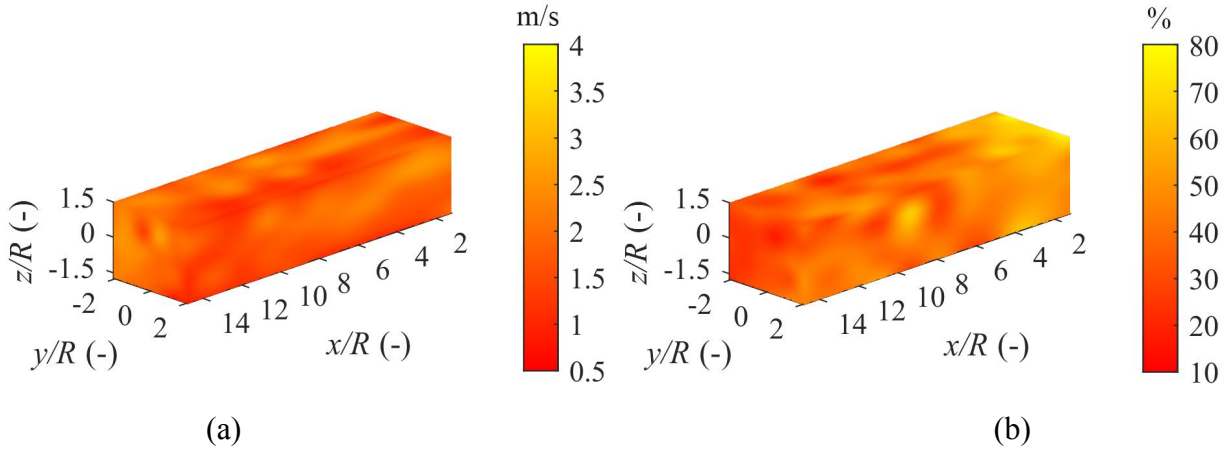

(a) (b)

Fig. 7. The generated wind field (a) Wind speed. (b) Turbulence intensity.

To reproduce a desired wind field for aerodynamic tests, three issues should be solved: (1) determining the testing position for the SWTM; (2) adjusting the center wind speed at the testing position to approximate the desired wind speed; (3) verifying the wind speed and the turbulence intensity at the rotor section.

Following the above track, the fans are set to work at a current frequency of 15.36 Hz at first. Then, a DANTEC Mini-CTA hot-wire anemometers with a probe (55P11) is used to measure the wind speed and the turbulence intensity of the whole wind field. 11×9 measuring point are arranged on the *YZ* plane and 12

measuring sections are set from x=1.2R to x=14.4R with an increments step of x=1.2R. The testing results are shown in Fig. 7.

As shown in Fig. 7 (a), the wind speed is almost the same when x is in the range of 3R~11R, but it tends to be unstable when x is greater than 7R. It can also be found from Fig. 7 (b) that, the wind field turbulence intensity becomes significantly high when x is less than 4R, and it tends to be unstable when x is greater than 6R. Hence, the testing position of the wind turbine is set at x=4.8R (where was set as a measuring section before). To generate the expect wind speed, the relationship between the center wind speed at the testing position and the current frequency of the fans is measured, and the result can be described as:

$$V = 0.1719 f \tag{9}$$

where f is the working current frequency of wind field generator. According to Eq. (9), the axial fans can generate a wind speed of 1.275 m/s when the current frequency is 7.42 Hz.

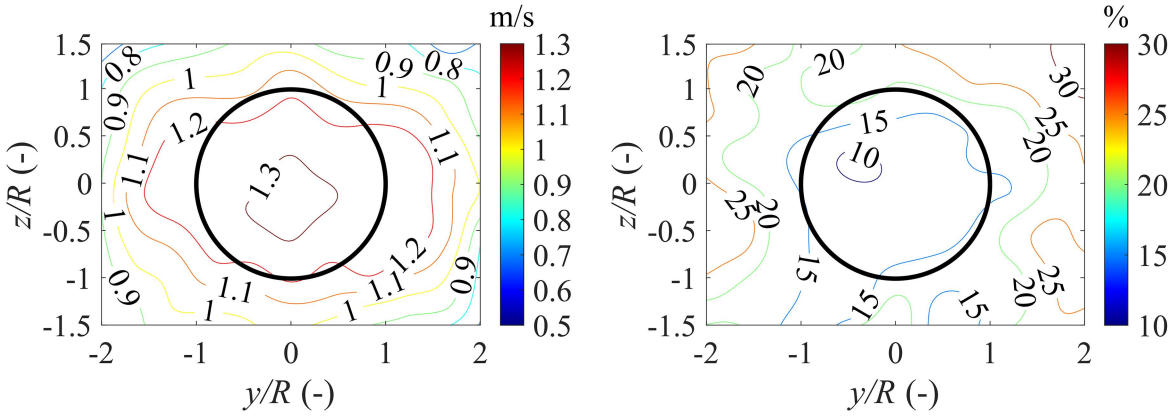

Fig. 8. The wind field on rotor section (a) Wind speed. (b) Turbulence intensity.

Finally, the wind speed and the turbulence intensity of the rotor section at the testing position are measured, and the results are shown in Fig. 8. Herein, the black circle represents the working area boundary of the rotor. It is obviously that, the wind speed and the turbulence intensity are stable in this working area. The average wind speed is 1.275 m/s, and the average turbulence intensity is 14%. According to Table 1, the average wind speed is equal to the desired wind speed. Besides, the reference turbulence intensity of the wind

experienced by a practical wind turbine is 12%~16% (IEC 2005). Hence, the wind field generator can reproduces the desired wind field.

2.4.2. Motions simulator

The floating platform of an OFWT has six kinds of motions under the real marine conditions, i.e. surge, pitch, sway, roll, heave, and yaw (Shokouhian et al. 2019, Tanaka et al. 2020, Wang et al. 2022). According to the existing studies (Jonkman and Musial 2010, Shin et al. 2014, Ma et al. 2021), the reference ranges of the above six kinds of motions at rated wind speed in RWT and SWTM can be calculated. The results are shown in Table 4.

Table 4 The motion range of floating platform in RWT and SWTM.

Motion Mode	RWT	SWTM
Surge	+9 m, -1 m	+1.125 m, -0.125 m
Pitch	+8°,0°	+8°,0°
Sway	+1 m, -2m	+0.125 m, -0.25m
Roll	+1°, 2°	+1°, 2°
Heave	1 m, -1 m	0.125 m, -0.125 m
Yaw	±2°	±2°

To reproduce the motions of floating platform, a 6-DOF motion platform with a dedicated control system is utilized as the motions simulator in this study. The motion simulator (TYT-D6B) is shown in Fig. 9. Its gross specifications are listed in Table 5. Obviously, the 6-DOF motion platform can satisfy the movement requirements of the SWTM. The motion simulator reproduces the dynamic responses of the floating platform by inputting the target motions to the dedicated soft control system. The target motions can be obtained by the

Table 5 Specifications of the 6-DOF platform.

Item	Specifications
Diameter of platform	1000 mm
Diameter of fixed base	1200 mm
Surge	+330 mm，-245 mm
Pitch	+28°，-25°
Sway	±260 mm
Roll	±20°
Heave	±174 mm
Yaw	±36°

simulation tools in coupling/decoupling conditions or from the exist research papers. It is worth noting that although damping is important for the analysis of the dynamic responses of OFWTs and its scaling factor can be obtained by the dimensional analysis. However, the motion simulator is directly reproducing the dynamic responses of floating platform in this paper. Thus, the scaling effect on damping is ignored.

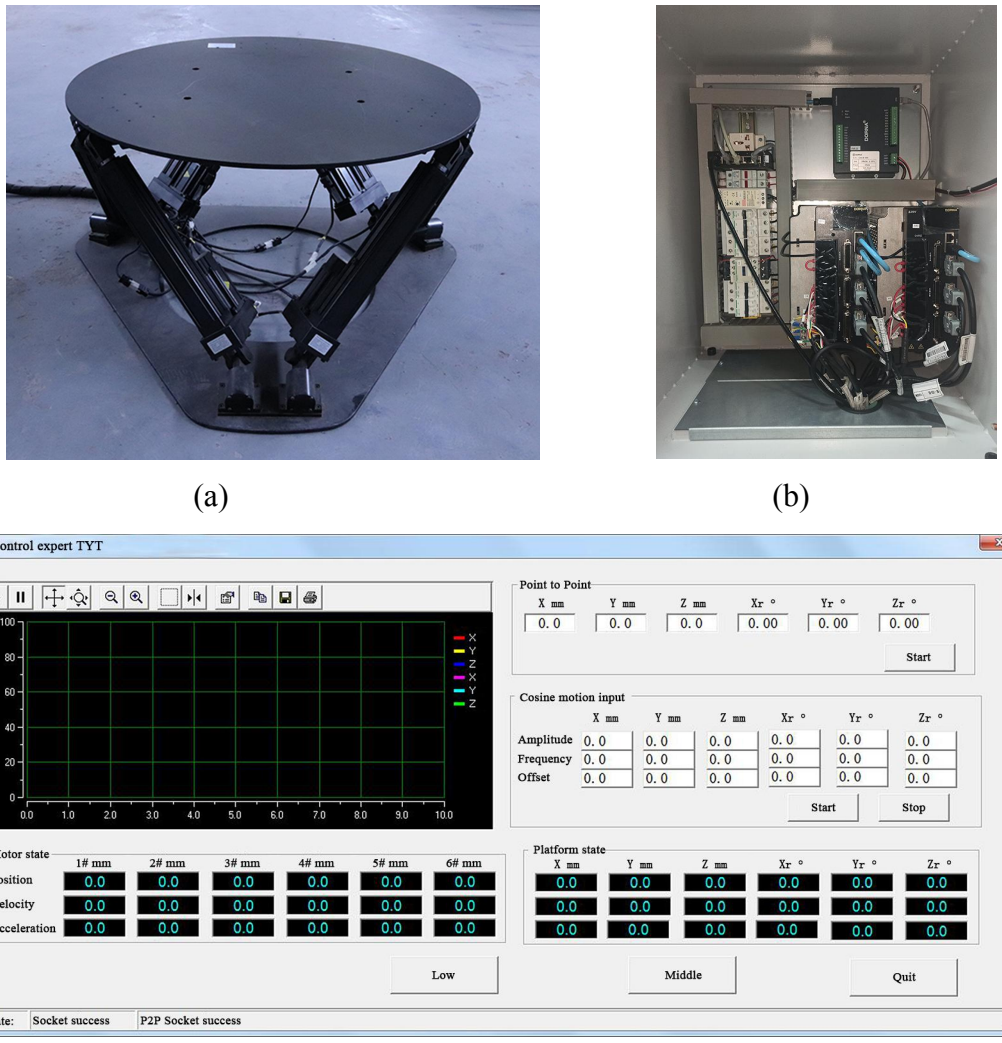

Fig. 9. The motion simulator (a) 6-DOF motion platform. (b) The dedicated hardware control system. (c) The dedicated software control system.

2.5. Fabrication of SWTM based aerodynamic testing apparatus

A SWTM based aerodynamic testing apparatus is fabricated and shown in Fig. 10. The fabricated parameters of the SWTM are shown in Table 6. In present study, the thrust is measured by a six-component load cell,

which is mounted at the bottom of the tower. The power is converted from the data measured by a torque sensor, which is installed inside the nacelle.

As can be seen from Table 6, the relative errors of all geometric factors are less than 4%. This means that the size of the SWTM reaches the design target. The relative error of the tower stiffness is -3.30%. In addition, the relative errors of the nacelle and tower mass are less than 5%. Therefore, it can be concluded that the designed SWTM can fully meets the aforementioned similarity requirements and scaling laws as well.

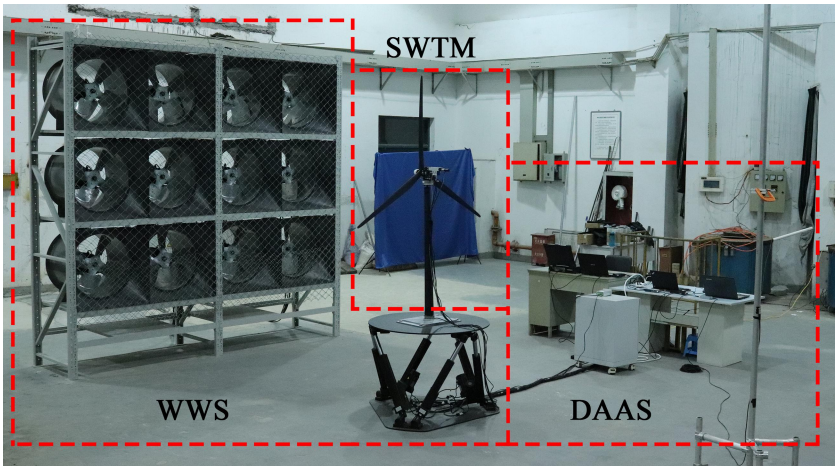

Fig. 10. The SWTM based aerodynamic testing apparatus.

Table 6 Measurement parameters and error rate of the SWTM.

Parameters	Target	SWTM	Relative error
Rotor diameter	1575 mm	1575 mm	0%
Hub diameter	43.75 mm	43.60 mm	-0.34%
Hub height	1125 mm	1167 mm	+3.73%
Tower length	1095 mm	1070 mm	-2.28%
Tower upper diameter	48.38 mm	48.75 mm	+0.76%
Tower lower diameter	75 mm	74.96 mm	-0.05%
Stiffness of tower	79.65 $N \cdot m^2$	77.02 $N \cdot m^2$	-3.30%
Nacelle mass	468.75 g	445.97 g	-4.86%
Tower mass	678.63 g	684.89 g	-0.92%

3. Aerodynamic tests

In this section, a series of preliminary experimental tests are carried out on the SWTM based aerodynamic testing apparatus. The aerodynamic performances of the fabricated SWTM without platform motions and with platform motions are tested consequently.

3.1. Aerodynamic test without platform motions

In these experiments, the tile angle is set as 5° (which is the design value of NREL-5MW RWT) and the 6-DOF platform is set to be stationary. The wind field is set as described in subsection 2.4.1. Fig. 11 shows the testing results and the relative errors of the thrust coefficients and the power coefficients. To avoid the possible influence of the negative power coefficients, the experimental TSR range is set as 5~8. As can be seen, the experimental data agree well with the theoretical data. More specifically, most of the relative errors of thrust coefficient at different TSRs are less than 5%, except that at TSR=6.5. Similarly, most of relative errors of power coefficient are less than 8%. There are only two outlier points of the relative errors in Fig.11 (b), i.e. the points at TSR=5 (with a relative error of -11.73%) and TSR=8 (with a relative error of 10.41%). The tiny deviations may be caused by the turbulence intensity of the wind flow, which was not considered during the analytical calculation.

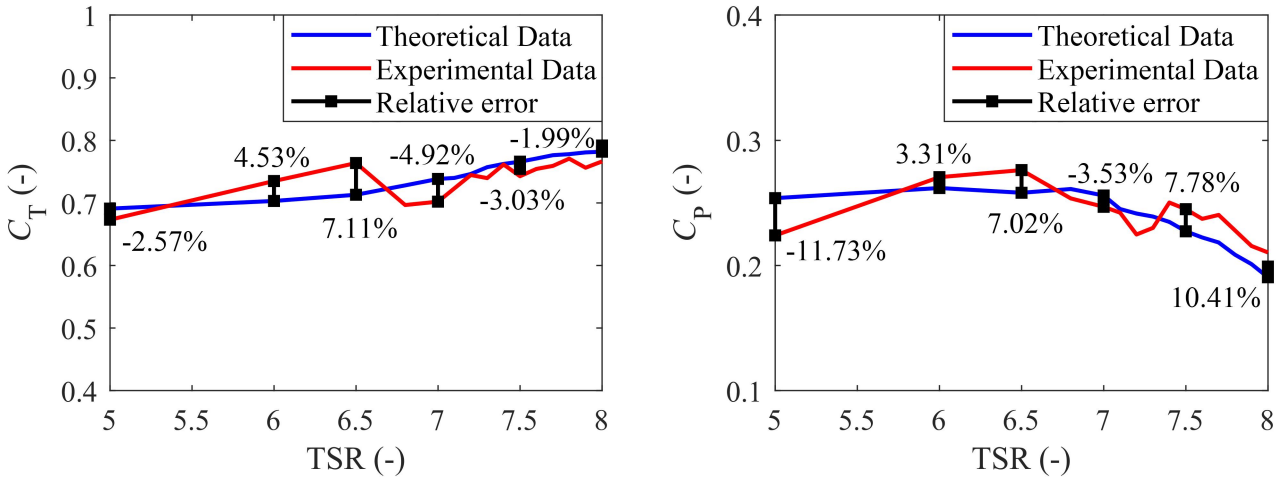

Fig. 11. Aerodynamic performance (a) The thrust coefficient. (b) The power coefficient.

To sum up, all the relative errors around the rated TSR are less than 10%. These results, once again, prove that the developed apparatus is reliable enough for carrying out aerodynamic performance tests.

3.2. Aerodynamic test with platform motions

Previous studies indicated that the motions of surge, pitch, and yaw have dominant effects on aerodynamics of OFWTs (Jonkman and Musial 2010, Stewart et al. 2012, Shin et al. 2014, Ma et al. 2021). Therefore, the present study will only tests the aerodynamic performance of the SWTM, which works at rated wind condition, experiencing the above three kinds of motions in decoupling mode. The tested thrust force is taken as the index to demonstrate the aerodynamic performance of the SWTM with platform motions. Referring to prior study (Sebastian and Lackner 2013), the frequencies of the three kinds of motions are set as 0.4Hz, while the amplitudes of the three kinds of motions are 50 mm, 5° and 5°,respectively. The time domain waveforms and the corresponding FFT spectrum of the model rotor thrust are illustrated in Fig. 12 and Fig. 13, respectively. For comparison convenience, the waveforms and FFT spectrum of the model rotor thrust with stationary platform are also provided.

As can be seen from Fig. 12 (a) and Fig. 13 (a), the rotor thrust in time domain is a periodic waveform. The fluctuating amplitude is 0.69N and the period is 0.5s. The 1P (the frequency of the rotor) signal component plays the main role followed by the 3P (the frequency of the blade) component in the FFT spectrum. As can be seen from Fig. 12 (b) and Fig. 13 (b), the time-domain waveform of rotor thrust under the surge motion demonstrates a stronger fluctuation (5.36N) and a longer period (2.5s) when compared with the stationary work condition. In the frequency domain, the surge-frequency related component is dominant while the 1P and 3P components are comparatively weak. As can be seen from Fig. 12 (c) and Fig. 13 (c), the time-domain waveform of rotor thrust under the pitch motion demonstrates a stronger fluctuation (2.19N) and a longer period (2.4s) when compared with the stationary work condition. In the frequency domain, the pitch-frequency related component is dominant though the 1P component can be clearly detected. As can be seen from Fig. 12 (d) and Fig. 13 (d), the time-domain waveform of rotor thrust under the yaw motion has a stronger fluctuation (0.79N) and a longer period (0.55s) when compared with the stationary work condition. In the frequency domain, the characteristic frequency of 1P is outstanding followed by an obvious

characteristic frequency related to the yaw motion, while the 3P frequency is not clearly detectable. In addition, a protruding component related to 2Hz is observed. Our further investigation reveals that this is the natural frequency of the SWTM structure.

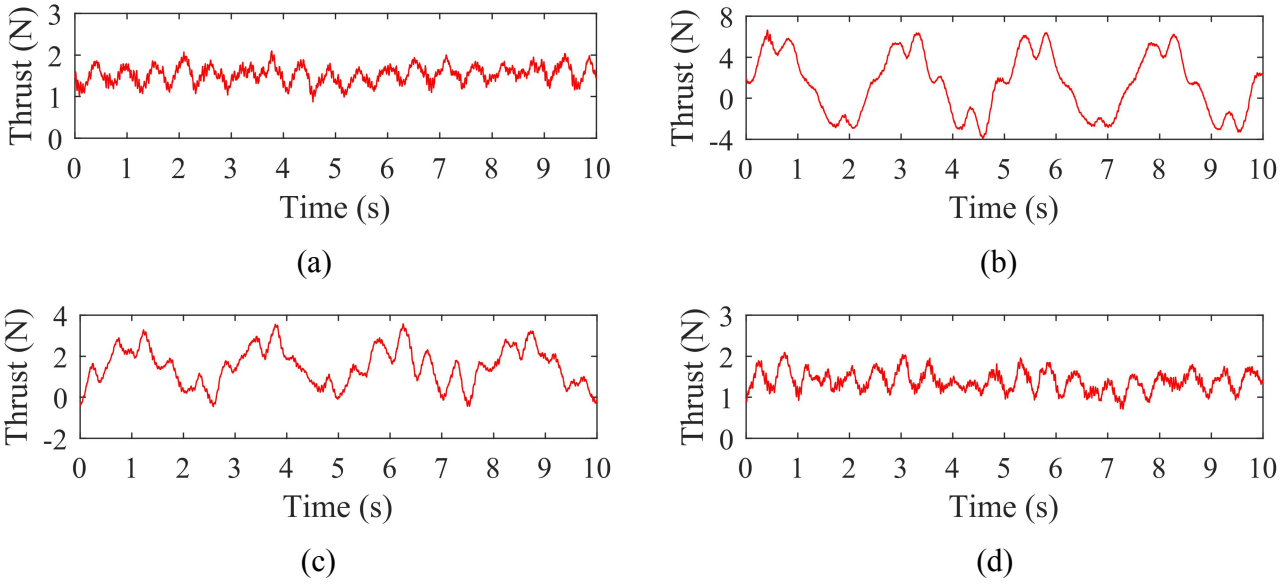

Fig. 12. Time domain waveforms of the model rotor thrust with different motion conditions (a) Stationary. (b) Surge. (c) Pitch. (d) Yaw.

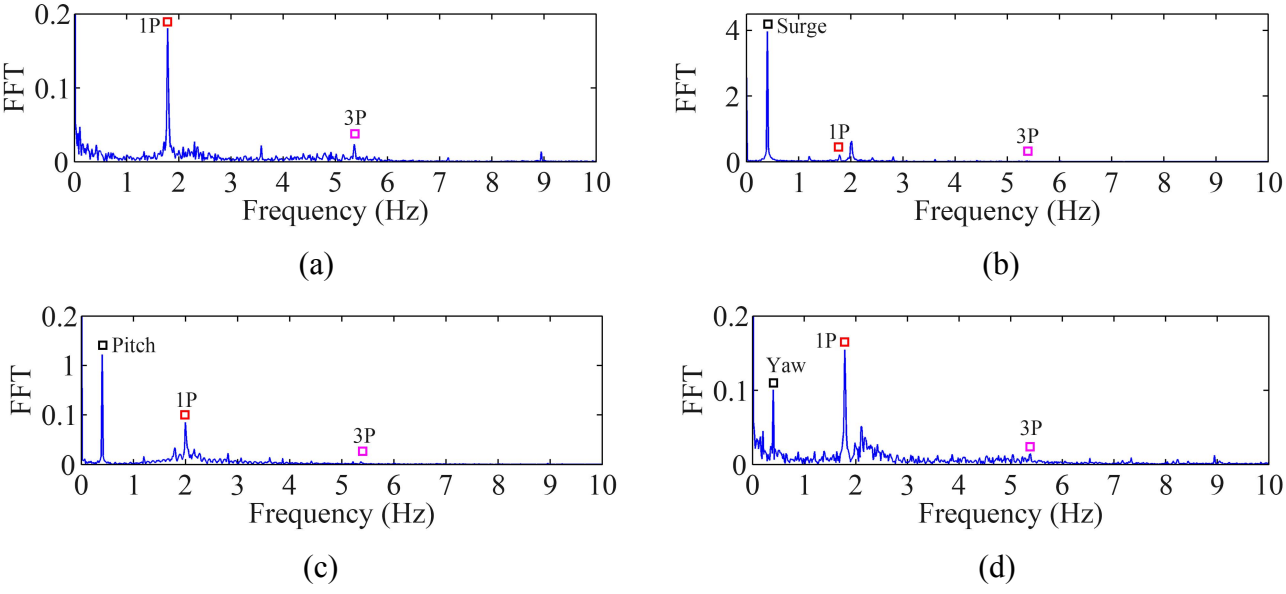

Fig. 13. FFT spectrum of the model rotor thrust (a) Stationary. (b) Surge. (c) Pitch. (d) Yaw.

Based on the above analyses, it can be found that the influences of surge, pitch, and yaw motions on the thrust performance decrease in turn. This can be explained by the following reason. For an OFWT, its

platform motions will bring periodical additional 'relative wind velocity' to the rotor. Among the platform motion induced relative wind velocity, the surge motion induced velocity is larger than those of pitch and yaw motions.

It is worth to note that the developed apparatus can also be used to investigate the coupling effects of time-varying inflow wind and platform motions on aerodynamics of the SWTM. This will be carried out in our next investigations.

4. Conclusions

This study presents an innovative SWTM based aerodynamic testing apparatus, which consists of an innovative SWTM, a WWS and a DAAS. The final conclusions of this study can be summarized as follows.

1) A SWTM with a double-deck tower and a redesigned blade is proposed. The double-deck tower can satisfies the design similarity requirements of geometry, stiffness and mass. The redesigned blade has a comparable aerodynamic performance at rated TSR with the blade of RWT.

2) The WWS consists of a wind field generator and a motion simulator, which can generate the desired wind field and the platform movements, respectively.

3) Several aerodynamic tests without platform motions are carried out to verify the effectiveness of this SWTM based aerodynamic testing apparatus. The testing results show that the aerodynamic performance of the SWTM is consistent with that of the RWT.

4) The rotor thrust of the SWTM experiencing platform motions is tested to reveal the unique influence of surge, pitch, and yaw motions on the aerodynamic performance. The influences of surge, pitch, and yaw motions on the thrust performance decrease in turn. The developed apparatus is expected to be beneficial for studying the dynamic aerodynamic characteristics of OFWTs.

Acknowledgments

The present work is sponsored by the National Natural Science Foundation of China (Grant no. 51875105).

Declaration of interest statement

The authors declare that they have no known competing financial interests or personal relationships that could have appeared to influence the work reported in this paper.

References

Ahn HJ, Shin H. 2019. Model test and numerical simulation of OC3 spar type floating offshore wind turbine. Int. J. Nav. Archit. Ocean Eng. 11 (1): 1–10.

Bayati I, Belloli M, Ferrari D, Fossati F, Giberti H. 2014. Design of a 6-DoF robotic platform for wind tunnel tests of floating wind turbines. Energy Procedia. 53: 313–323.

Belloli M, Bayati I, Facchinetti A, Fontanella A, Giberti H, Mura FL, Taruffi F. 2020. A hybrid methodology for wind tunnel testing of floating offshore wind turbines. Ocean Eng. 210: 107592.

Chen J, Hu Z, Wan D, Xiao Q. 2018. Comparisons of the dynamical characteristics of a semi-submersible floating offshore wind turbine based on two different blade concepts. Ocean Eng. 153: 305–318.

Du W, Zhao Y, He Y, Liu Y. 2016. Design, analysis and test of a model turbine blade for a wave basin test of floating wind turbines. Renew. Energy. 97: 414–421.

Duan F, Hu Z, Liu G, Wang J. 2016a. Experimental comparisons of dynamic properties of floating wind turbine systems based on two different rotor concepts. Appl. Ocean Res. 58: 266–280.

Duan F, Hu Z, Niedzwecki JM. 2016b. Model test investigatiaon of a spar floating wind turbine. Mar. Struct. 49: 76–96.

Fowler MJ, Kimball RW, Thomas DA, Goupee AJ. 2013. Design and testing of scale model wind turbines for use in wind/wave basin model tests of floating offshore wind turbines. Proceedings of the International Conference on Offshore Mechanics and Arctic Engineering.

Goupee AJ, Koo B, Kimball RW, Lambrakos KF, Dagher HJ. 2012. Experimental comparison of three floating wind turbine concepts. Proceedings of the International Conference on Offshore Mechanics and Arctic Engineering - OMAE.

IEC. 2005. Wind Turbines - Part 1: Design requirements. International Electromechanical Commission (IEC).

Jonkman J, Butterfield S, Musial W, Scott G. 2009. Definition of a 5-MW reference wind turbine for offshore system development. National Renewable Energy Laboratory.

Jonkman J, Musial W. 2010. Offshore Code Comparison Collaboration (OC3) for IEA Task 23 Offshore Wind Technology and Deployment.

Li C, Ye Z, Gao W, Jiang Z. 2013. Modern Large-scale Wind Turbine Design Principle. Shanghai Scientific & Technical Publishers; p. 102-138.

Lin J, Wang Y, Duan H, Zhang J. 2022a. Optimization Design of Blades for a Scaled Offshore Floating Wind Turbine. Proceedings of the 2021 International Conference on Mechanical Design. Mechanism and Machine Science. 111: 189-201.

Lin J, Duan H, Xu B, Wang Y, Zhang J. 2022b. Equivalent Aerodynamic Design of Blade for Offshore Floating Wind Turbine Model. J. Mar. Sci. Eng. 10 (2): 1–13.

Lin J. 2022c. Design of a Large Scaled Model of Offshore Floating Wind Turbine and Optimization of its Key Components. Fuzhou: Fuzhou University.

Liu Y, Li S, Chan PW, Chen D. 2019. On the failure probability of offshore wind turbines in the China coastal waters due to typhoons: A case study using the OC4-Deep C wind semisubmersible. IEEE Trans. Sustain. Energy. 10 (2): 522–532.

Ma Y, Chen C, Fan T, Yan X, Lu H. 2021. Research on motion inhibition method using an innovative type of mooring system for spar floating offshore wind turbine. Ocean Eng. 223: 108644.

Martin HR. 2011. Development of a scale model wind turbine for testing of offshore floating wind turbine systems. Maine: University of Maine.

Martin HR, Kimball RW, Viselli AM, Goupee AJ. 2014. Methodology for Wind/Wave Basin Testing of Floating Offshore Wind Turbines. J. Offshore Mech. Arct. Eng. 136(2): 020905.

Nielsen FG, Hanson TD, Skaare B. 2006. Integrated dynamic analysis of floating offshore wind turbines. European Wind Energy Conference and Exhibition 2006.

Porté-Agel F, Bastankhah M, Shamsoddin S. 2020. Wind-Turbine and Wind-Farm Flows: A Review. Boundary-Layer Meteorol. 174 (1): 1–59.

Robertson A, Jonkman J, Masciola M, Song H. 2014. Definition of the Semisubmersible Floating System for Phase II of OC4.

Ruzzo C, Muggiasca S, Malara G, Taruffi F, Belloli M, Collu M, Li L, Brizzi G, Arena F. 2021. Scaling strategies for multi-purpose floating structures physical modeling: state of art and new perspectives. Appl. Ocean Res. 108: 102487.

Sebastian T, Lackner, MA. 2013. Characterization of the unsteadyaerodynamics of offshore floating wind turbines. Wind Energy. 16:339–352.

Shin H, Lee W, Jung K, Kim J. 2014. Model test and simulation of modified spar type floating offshore wind turbinae with three catenary mooring lines. J. Renew. Sustain. Energy. 6 (4): 1-24.

Shokouhian M, Head M, Seo J, Schaffer W, Adams G. 2019. Hydrodynamic response of a semi-submersible platform to support a wind turbine. J. Mar. Eng. Technol. 20 (3): 170-185.

Simandjuntak S, Bausch N, Farrar A, Ahuir-Torres IJ, Thomas B, Muna J. 2021. iWindCr field trial and electrochemical analysis for corrosion detection and monitoring offshore wind turbine's MP-TP steel components. J. Mar. Eng. Technol. 21 (6): 311-323.

Stewart GM, Lackner MA, Robertson A, Jonkman J, Goupee AJ. 2012. Calibration and validation of a fast floating wind turbine model of the deepcwind scaled tension-leg platform. Proceedings of the International Offshore and Polar Engineering Conference.

Tanaka K, Sato I, Utsunomiya T, Kakuya H. 2020. Validation of dynamic response of a 2-MW hybrid-spar floating wind turbine during typhoon using full-scale field data. Ocean Eng. 218: 108262.

Tchertchian N, Millet D. 2022. Which eco-maintenance for renewable energy? A simulation model for optimising the choice of offshore wind farm maintenance vessel. J. Mar. Eng. Technol https://doi.org/10.1080/20464177.2022.2044584.

Wang Y, Lin J, Zhang J. 2022. Investigation of a new analytical wake prediction method for offshore floating wind turbines considering an accurate incoming wind flow. Renew. Energy. 185: 827–849.

Wen B, Zhang Q, Tian X, Peng ZK. 2019. An Experimenttal Apparatus for Investigating The Unsteady Aerodynamics of a Floating Wind Turbine. Proceedings of the ASME 2019 38th International Conference on Ocean, Offshore and Arctic Engineering.

Wen B, Tian X, Dong X, Li Z, Peng Z. 2020. Design approaches of performance-scaled rotor for wave basin model tests of floating wind turbines. Renew. Energy. 148: 573–584.

Yang J, He Y, Zhao Y, Shao Y, Han Z. 2021. Experimental and numerical studies on the low-frequency responses of a spar-type floating offshore wind turbine. Ocean Eng. 222: 108571.

Yang JM, Xiao LF, Sheng ZB. 2008. Experimental Study on Hydrodynamics of Marine Engineering. Shanghai: Shanghai JiaoTong University Press; p. 53-72.

Table Caption List

Figure Captions List